Journal of Alloys and Compounds 509 (2011) 3859–3865

Contents lists available at ScienceDirect

Journal of Alloys and Compounds

journal homepage: www.elsevier.com/locate/jallcom

On the sol–gel synthesis and structure, optical, magnetic and impedance behaviour of strontium cobaltite powder

Shivendra Kumar Jaiswal, Jitendra Kumar*

Materials Science Programme, Indian Institute of Technology Kanpur, Kanpur 208016, India

ARTICLE INFO

Article history:
Received 6 May 2010
Received in revised form
15 December 2010
Accepted 17 December 2010
Available online 24 December 2010

Keywords:
Sol–gel synthesis
Optical absorption
Impedance analysis
Strontium cobaltite

ABSTRACT

An attempt has been made to synthesize strontium cobaltite powder by a sol–gel process using strontium and cobalt nitrates as precursors and characterize that with regard to formation, optical absorption, magnetic behaviour, and impedance characteristics. The synthesis process involves gel formation, digestion for 4 h, drying at 150 °C for 24 h, and calcination at 1000 °C for 10 h in air. The product is shown to contain dumbbell shape particles and correspond to a rhombohedral phase that matches well with the composition $Sr_6Co_5O_{15}$, lattice parameters $a = 6.869$ Å, $\alpha = 87.543°$, $Z = 1$, and space group R32 with ~7 wt% of a secondary phase of spinel cubic Co_3O_4 ($a = 8.0862$ Å). The optical absorption exhibits peaks at 4.12, 1.90, 1.58, 1.23 and 0.87 eV which are attributed to charge transfer transitions involving oxygen and/or cobalt ions and Co^{3+} d–d transitions. Further, the sample appears to be weakly ferromagnetic with two Curie temperatures (T_C) as 750 and 790 K, coercivity of 70 Oe and remanent magnetization $\sim 9 \times 10^{-4}$ emu/g. Impedance characteristics over a wide frequency range of 20 Hz–2 MHz at 131–350 K reveal contributions from two parallel 'RC' circuits belonging to bulk and grain boundaries with the later displaying significant space charge polarization, the relaxation time of which decreases with increase of temperature (range being 5–32 μs).

1. Introduction

The salient feature of perovskite-cubic based oxides $ABO_{3-\delta}$ (A = La, Sr, Ba; B = Co, Fe, etc.) is their ability to accommodate (i) a wide range of oxygen deficiency and (ii) mixed oxidation states of transition metal at B-sites. The diffusion of oxygen via vacancies and electron jump from B^{n+} to $B^{(n+1)+}$ ions connected through O-2p orbitals allow them to exhibit mixed conductivity [1,2]. Also, their electrical, magnetic and other physico-chemical properties can be controlled by synthesis route, experimental conditions and varying compositions [1–3]. The compounds revealing excellent oxygen permeation characteristics have either a fluorite- or perovskite-type cubic structure [1,4]. They have found widespread applications in inorganic membranes, oxygen pumps, solid oxide fuel cells, oxidative coupling of methane as catalyst, gas sensors, automotive gas exhaust analysis, combustion control, electrochemical reduction of nitrous oxide and optical sensor [4–15]. An important member of this family is the strontium cobaltite ($SrCoO_{3-\delta}$) which displays reasonable oxygen non-stoichiometry and crystallizes in several phases (e.g., orthorhombic, rhombohedral and cubic) depending on the synthesis route and thermal treatment involved (Section 3.1). Also, the cubic $SrCoO_{2.75}$ (space group Pm3m) and tetragonal $SrCoO_{2.82}$ (space group I4/mmm) phases (termed as intermediate vacancy structures) have been observed [16]. The synthesis at high-pressure (~6 GPa) produces $SrCoO_3$ (i.e., $\delta = 0$) phase with perovskite-type cubic structure [17]. It shows order–disorder phenomenon of oxygen vacancies above 910 °C leading thereby to (i) significant enhancement in the anion permeation (oxygen ion conductivity being 2.5 Ω^{-1} cm^{-1} at 900 °C, activation energy 31 kJ/mol) and (ii) semiconducting to metallic transition [18]. A phase transformation observed via neutron diffraction above 250 °C in orthorhombic $SrCoO_{2.5}$ is accompanied by significant increase in conductivity and attributed to reduction in certain Co–O bond lengths. Subsequent transformation above 500 °C to hexagonal structure, however, causes decrease in conductivity. Above 900 °C, conductivity increases again (maximum value being 150 Ω^{-1} cm^{-1}) and the sample exhibits perovskite cubic structure, characterized by a three dimensional vertex-sharing network of CoO_6 octahedra and metallic behaviour (i.e., decrease of conductivity with increase of temperature) [19]. Tapiline et al. [20] have investigated the electronic structures of $SrCoO_{3-\delta}$ ($\delta = 0$, 0.125,0.25) compounds using density functional theory under spin polarized local density approximation (SLDA) and revealed two types of vacancy ordering with energies 0.22 and 0.01 eV. The strontium cobaltite is reported to be ferromagnetic in nature with Curie temperature of 222 or 290 K [21,22]. On the other hand, $SrCoO_{3-\delta}$ ($\delta = 0.5$ or $Sr_2Co_2O_5$) phase depicts antiferromagnetism with Neel temperature of 545 K or 570 K [23,24]. The magnetic

* Corresponding author. Tel.: +91 512 2597107; fax: +91 512 2597664.
E-mail address: jk@iitk.ac.in (J. Kumar).

0925-8388/$ – see front matter © 2010 Elsevier B.V. All rights reserved.
doi:10.1016/j.jallcom.2010.12.125

nature in fact depends on oxygen stoichiometry and relative amounts of Co^{3+} and Co^{4+} ions with their spin states high, intermediate or low. Another series of cobalt deficient composition $(A_3Co_2O_6)_m(A_3Co_3O_9)_n$ [A = Ba, Sr, Ca with m, $n \geq 1$] consists of pseudo-one dimensional structure with CoO_6 polyhedra (octahedra and triangular prisms) forming Co–O chain by sharing their faces [25,26]. $Sr_6Co_5O_{15}$ is a member of the series with $m = n = 1$ in which four consecutive CoO_6 octahedra and one CoO_6 triangular prism form Co–O chains in the rhombohedral unit cell and cobalt species exist in both 3+ and 4+ oxidation states. Iwasaki et al. [27] have investigated the electrical resistivity (ρ), Seebeck coefficient (S) and power factor (S^2/ρ) of cobalt deficient $Sr_6Co_5O_{15}$ phase in the temperature range 23–850 °C. Accordingly, it shows semiconducting behaviour with ρ in the range 0.13–8 Ω-cm, positive Seebeck coefficient of 110–138 μV/K, and maximum power factor of 1.4×10^{-5} W/mK^2. By treating at different temperatures (500–850 °C), it transforms into oxygen deficient rhombohedral phase with composition $Sr_6Co_5O_{15-\delta}$; δ varying up to $\delta = 0.74$ [28]. The unit cell parameters on hexagonal axes vary with decreasing oxygen content, i.e., while a-parameter increases, c-parameter decreases [28]. Based on molecular orbital calculations, Whangbo et al. [29] suggested presence of polyhedral chains with four non-magnetic Co^{4+} (d^5) ions in the octahedral sites (Co–Co distance being 2.53 and 2.36 Å) and one magnetic Co^{2+} (d^7) ion (with $S = 1/2$ or 3/2) in the trigonal prism. The values of heat capacity and entropy of $Sr_6Co_5O_{15}$ estimated theoretically in the temperature range 100–1300 K on the basis of first principles lie in the range of 5.92–32.01 J/mol/K and 2.22–56.26 J/mol/K, respectively [30]. The single crystal of oxygen deficient strontium cobaltite of composition $Sr_6Co_5O_{14.3}$ grown by a flux method is shown to contain one dimensional columns of Co–O octahedra and triangular prism, exhibiting rhombohedral phase with space group R3 and lattice parameters based on hexagonal axes as $a = 9.4334(6)$ Å, $c = 12.5156(6)$ Å [31].On the other hand, single crystals of $Sr_6Co_5O_{14.7}$ and Ni-doped compound of composition $Sr_6Ni_{0.1}Co_{4.9}O_{14.36}$ correspond to a different space group $R\bar{3}$ and lattice parameters $a = 9.459(1)$ Å, $c = 12.469(2)$ Å and $a = 9.440(1)$ Å, $c = 12.476(3)$ Å, respectively [32]. The structure can be described by distribution of two sets of oxygen polyhedra; four octahedra (with Co^{4+} ions) plus one trigonal prism (with Co^{2+} ions) and three octahedra (with Co^{4+} ions) plus two intermediate polyhedral (with Co^{2+} ions). The single crystal of $Sr_6Co_5O_{14.3}$ exhibits electrical conductivity (σ) an order of magnitude higher while power factor (S^2/ρ) ~ 30 times larger than the polycrystalline $Sr_6Co_5O_{15}$; the value of σ varies 260–9600 Ω^{-1} m^{-1} when the temperature is raised from 300 to 900 K and of 'S^2/ρ' is 2.0×10^{-5} W m^{-1} K^{-2} [27,33]. Further, it shows antiferromagnetic nature with Neel temperature of 25 K, Curie constant ~3.88 emu K mol^{-1} and Weiss constants −25 K, respectively [32]. Recently, Takami et al. [34] have synthesized nano-sized $Sr_6Co_5O_{15}$ compound by solid state sintering method, subjected to milling to further reduce size from 409 to 102 nm and studied their resistivity and thermoelectric power. The cobalt oxide-based materials are also known to be potential candidate for the thermoelectric devices at elevated temperatures [3,32–35]. Numerous investigations on strontium cobaltite of different compositions so far involved synthesis by solid state sintering of oxides and/or salts at elevated temperatures for long duration [27,28,33]. However, inhomogeneity and phase(s) stability in resulting samples continue to cause uncertainty in results and their possible correlation. As a consequence, their behaviour is still not fully understood. Sol–gel synthesis is yet another route which offers a number of advantages, e.g., homogeneous mixing of precursor constituents at atomic level, better stoichiometry control, high purity, and low cost. Attempt has therefore been made here to (i) synthesize strontium cobaltite via oxalate based sol–gel route for the first time and (ii) reinvestigate its formation, optical absorption, magnetic behaviour, and impedance characteristics.

2. Experimental

Strontium cobaltite powder was synthesized by a sol–gel process using $Sr(NO_3)_2$, $Co(NO_3)_2{\cdot}6H_2O$ and oxalic acid as precursors and ethanol as a solvent. Due to poor solubility of $Sr(NO_3)_2$ in ethanol, distilled water was added drop wise to achieve complete dissolution. After mixing the nitrate salt solutions of appropriate stoichiometry, oxalic acid solution was added to form a gel which, in turn, was digested first for 4 h and then dried at 150 °C for 24 h. The product was later subjected to calcination in air at 1000 °C for 10 h after sieving through a 240 mesh. The resulting black powder was characterized for phase(s), morphology, magnetic properties and optical absorption using a Rich Seifert X-ray diffractometer model ISO Debye flux 2002, a scanning electron microscope (FEI Quanta 200 HV), a vibrating sample magnetometer (Princeton VSM model-150) and a UV-Vis-NIR spectrophotometer (Varian Cary 5000), respectively.

Also, the impedance measurements were performed on a pellet (size 10 mm diameter and thickness 1.5 mm) using a HP LCZ meter model 4192 in wide frequency range 20 Hz–2 MHz at 131–350 K.

3. Results and discussion

3.1. Formation of strontium cobaltite

X-ray diffraction (XRD) pattern of the stable compound obtained after calcination of the dried sol–gel product at 1000 °C for 10 h in air is shown in Fig. 1. Its analysis reveals the presence of a $Sr_6Co_5O_{15}$ phase having a $Ba_6Ni_5O_{15}$-type trigonal structure, space group R32, with lattice parameters on the hexagonal axes as $a = 9.5035(2)$ Å, $c = 12.3966(4)$ Å, $Z = 3$ [36,37]; the corresponding rhombohedral unit cell dimensions being $a = 6.869$ Å, $\beta = 87.543°$, $Z = 1$. Table 1 lists the 2θ's, d-spacings, relative intensities, and $h\,k\,l$ values of various diffraction peaks. Since the amounts of precursors have been taken to yield $SrCoO_{3-\delta}$ (compound is usually oxygen deficient), another minor phase containing the remaining cobalt is also expected to be present. Thus, there can be two possibilities depending upon the secondary oxide phase as CoO or Co_3O_4. The balanced reaction can therefore be written as

$$6\,SrCoO_{3-\delta} \rightarrow Sr_6Co_5O_{15} + CoO; \quad \text{if } \delta = 1/3$$

or

$$18\,SrCoO_{3-\delta} \rightarrow 3Sr_6Co_5O_{15} + Co_3O_4; \quad \text{if } \delta = 5/18$$

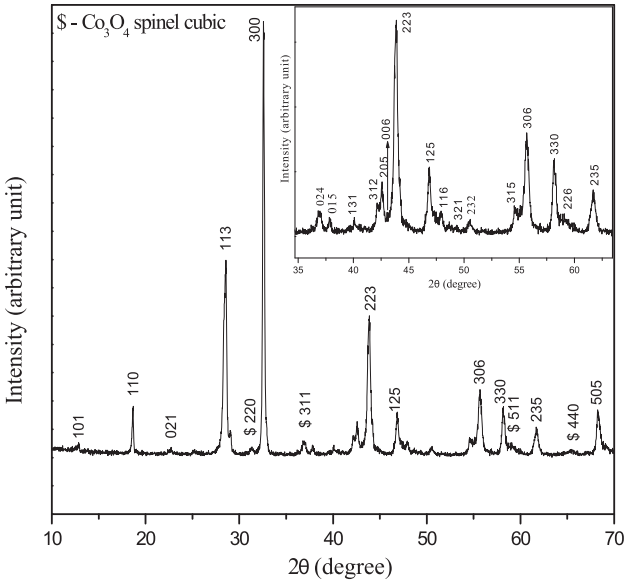

Fig. 1. X-ray diffraction patterns of dried sol–gel product after calcination at 1000 °C in air for 10 h. The inset shows the zoom view of the portion between (2θ) 35° and 65°.

Table 1
The 2θ's, d-spacings, relative intensities, $h\,k\,l$ values of various diffraction peaks.

S. no.	2θ (deg.)	I/I_o	d(Å) obs	d(Å)[a] cal	$h\,k\,l$[a]	$h\,k\,l$[b]
1	12.856	2	6.879	6.857	101	
2	18.673	11	4.748	4.752	110	
3	22.601	1	3.931	3.906	021	220
4	25.139	<1	3.539	–	–	
5	28.578	45	3.121	3.118	113	311
6	29.050	5	3.070	–	–	511
7	31.350	1	2.850	–	–	
8	32.581	100	2.746	2.743	300	440
9	36.801	3	2.440	2.476	024	
10	37.027	4	2.425	–	–	
11	37.804	2	2.377	2.373	015	
12	40.081	2	2.247	2.245	131	
13	42.141	4	2.142	2.142	312	
14	42.577	8	2.120	2.124	205	
15	43.041	3	2.099	2.066	006	
16	43.879	32	2.062	2.059	223	
17	46.859	10	1.937	1.939	125	
18	47.920	3	1.896	1.895	116	
19	48.679	1	1.866	1.867	321	
20	50.557	2	1.804	1.805	232	
21	54.560	4	1.681	1.679	315	
22	55.602	13	1.652	1.650	306	
23	58.178	10	1.584	1.584	330	
24	59.084	3	1.562	1.559	226	
25	61.681	6	1.503	1.502	235	
26	65.600	1	1.421	–	–	
27	68.241	10	1.373	1.371	505	

[a] $Sr_6Co_5O_{15}$ trigonal, space group R32, $Z=3$, lattice parameters on hexagonal axes as $a=9.5035(2)$ Å, $c=12.3966(4)$ Å [36]; JCPDS File# 49-0692.
[b] Co_3O_4 spinel cubic with $a=8.0862(4)$ Å, space group $Fd\bar{3}m$ [36]; JCPDS File# 09-418.

Examining the XRD pattern closely, additional weak lines do correspond to Co_3O_4 (Table 1), consistent with the other report [36]. Accordingly, the composition of original product becomes $SrCoO_{2.72}$ (i.e., $\delta=5/18$) with ~7 wt% of Co_3O_4. In contrast to stoichiometry $SrCoO_3$ where cobalt is tetravalent, $Sr_6Co_5O_{15}$ contains either two Co^{3+} and three Co^{4+} ions or one Co^{2+} and four Co^{4+} ions to ensure charge neutrality. In both the cases, the average charge on cobalt turns out to be 3.6. If oxygen content deviate, the relative number of Co^{4+} and Co^{3+} or Co^{2+} ions is expected to differ some what. Similarly, Co_3O_4 is comprised of Co^{2+} and Co^{3+} ions. The various oxygen deficient phases encountered in $SrCoO_{3-\delta}$ powder synthesized with different processing routes and conditions (e.g., calcination temperature, cooling step, environment–oxygen, nitrogen, air, argon) can be summarized as follows:

The product synthesized by mixture of $SrCO_3$ and Co_3O_4 powders in air above 900 °C and rapidly quenched to room temperature exhibits a brownmillerite ($4CaO{\cdot}Fe_2O_3{\cdot}Al_2O_3$)-type orthorhombic structure with lattice parameters $a=5.57$ Å, $b=15.7$ Å, $c=5.46$ Å, space group Icmm [38,39] and ordered anionic vacancies. Further, it contains CoO_6 octahedra and CoO_4 tetrahedra in alternating layers along the b-axis. The structure is related to perovskite $SrCoO_{3-\delta}$ -cubic phase ($a_o \sim 3.84$ Å), such that $a \sim a_o\sqrt{2}$, $b \sim 4a_o$ and $c \sim a_o\sqrt{2}$. But above 900 °C, $SrCoO_{3-\delta}$ exhibits Co^{4+} containing tetragonal phase in oxygen atmosphere, perovskite-type cubic at high pressure and orthorhombic under ambient condition [38]. Also, samples crystallize in a $BaNiO_3$-type 2H-hexagonal cell when synthesized below 900 °C. Grenier et al. [40] worked out the lattice parameters for brownmillerite-type orthorhombic phase of $SrCoO_{2.5}$ as $a=5.456$ Å, $b=15.664$ Å, $c=5.556$ Å, $Z=8$, space group Imma or I2mb and attributed its stabilization to the high spin state (HS) of Co^{3+} ions. By heating $SrCoO_{2.5}$ in nitrogen atmosphere at 750 °C, a rhombohedral phase emerges with lattice parameter $a=6.853(1)$ Å, $\alpha=86.90°$, $Z=3$, space group R $\bar{3}$ m or subgroup, ~11% reduced volume, and Co^{3+} ions of reduced radii because of assuming intermediate state between high (HS) and low spin (LS) configuration [41]. Harrison et al. [36] identified this product as cobalt deficient with composition $Sr_6Co_5O_{15}$ and trigonal $Ba_6Ni_5O_{15}$-type structure with lattice parameters on hexagonal axes $a=9.5035(2)$ Å, $c=12.3966(4)$ Å, $Z=3$, and space group R32. It contains SrO_3 layers in close-packed arrangement with cobalt ions occupying fraction of voids and forming three sets of four CoO_6 octahedra and one CoO_6 trigonal prism (sharing faces). According to Takeda et al. [42], $SrCoO_x$ crystallizes in brownmillerite or perovskite-type cubic phases depending upon the oxygen content (x) $2.42 < x < 2.52$ or 2.29. The mixture of two phases result for composition having 'x' in between 2.30 and 2.42. Further, annealing of brownmillerite phase under high oxygen pressure at 300 °C gives perovskite-type cubic phase of composition $x=2.67$–2.80 [42]. Vashook et al. [43] have detected three polymorphs of $SrCoO_{2.5-\delta}$; the rhombohedral ($\delta \leq 0.16$), pseudo-perovskite cubic comprising of microdomains ($0.16 \leq \delta \leq 0.21$) and ordered perovskite cubic ($\delta \geq 0.21$) phases. Temperature dependent neutron powder diffraction studies of brownmillerite-type $SrCoO_{2.5}$ showed its transformation to (i) rhombohedral phase with lattice parameters on hexagonal axes as $a=9.5257(4)$ Å, $c=12.6405(9)$ Å between 530 °C and 588 °C and (ii) perovskite-type cubic phase with $a=3.9667(3)$ Å at 882 °C [44]. Iwasaki et al. [28] synthesized non-stoichiometric $Sr_6Co_5O_{15.12}$ and $Sr_6Co_5O_{15-\delta}$ ($\delta=0.02, 0.55, 0.74$) compounds by solid state reaction of $SrCO_3$ and Co_3O_4 powder in air and observed phase stability of $Sr_6Co_5O_{15}$ in the temperature range 873–973 K and structural transitions at 773K and 1023 K. With loss of oxygen, decrease of 'a' and increase of 'c' occur in the progressive manner. The increase in 'c' parameter is caused by increase in Co–Co distance between the CoO_6 trigonal prism and CoO_6 octahedron.

3.2. Morphology

Fig. 2 shows a few typical scanning electron micrographs recorded in secondary electron (SE) mode of the product at various stages of synthesis. The gel dried at 150 °C for 24 h shows small sticks of various sizes (Fig. 2a). The dried gel product (when ground and heated at a rate of 4 °C/min up to 800 °C, cooled immedi-

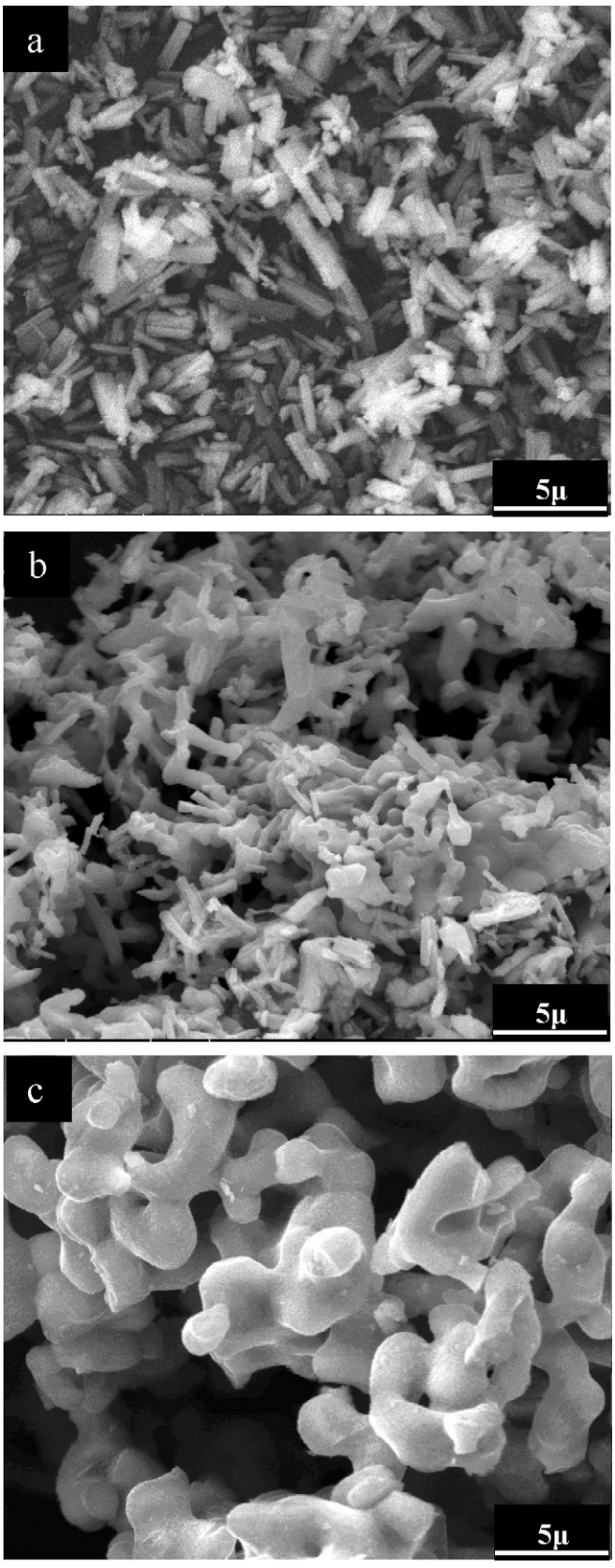

Fig. 2. Scanning electron micrographs (SE mode) of sol–gel product after (a) drying at 150 °C for 24 h, (b) heating at a rate of 4 °C/min up to 800 °C following drying step and then cooling to room temperature, (c) formation of strontium cobaltite at 1000 °C.

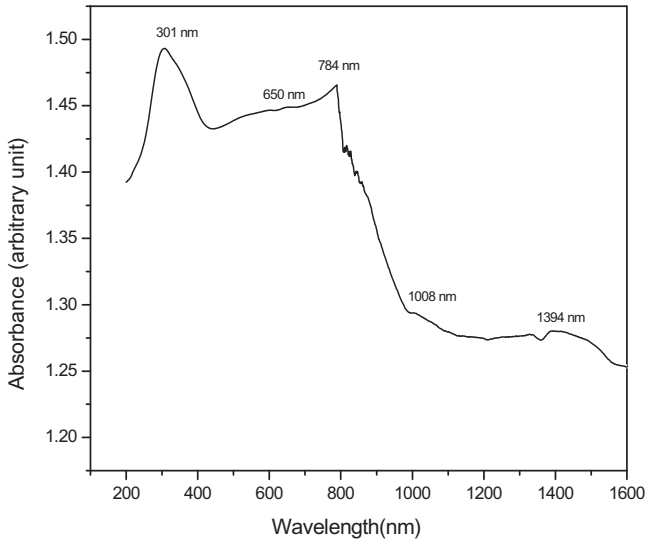

Fig. 3. Optical absorption spectrum of strontium cobaltite.

ately at a rate of 10 °C/min. to 400 °C and furnace cooled thereafter to room temperature) assumes jig-jag assembly of bonded sticks or coral reef-like morphology (Fig. 2b). The ground dried product after heating at 1000 °C for 10 h, and cooling (first at a rate 4 °C/min up to 400 °C, and then in furnace to room temperature) depicts dumbbell-like micrometer size particles of strontium cobaltite (Fig. 2c).

3.3. Optical absorption

Fig. 3 shows the optical absorption spectrum of the strontium cobaltite powder in the wavelength range of 200–1600 nm. It contains two major peaks at wavelengths of 301 nm (4.12 eV) and 784 nm (1.58 eV) and other minor peaks at 650 nm (1.90 eV), 1008 nm (1.23 eV), and 1394 nm (0.87 eV) with a few more in the range 800–1000 nm (1.55–1.24 eV). There is no report available in the literature for optical absorption of $SrCoO_{3-\delta}$. The spectrum can be explained in terms of charge transfer and/or crystal field transitions similar to those occurring in transition metal (TM) oxides. In the latter, the valence band of 2p-oxygen is separated from empty 4s-TM band by an energy gap of 4–6 eV. The interactions of 3d-TM electrons with the surrounding oxygen ions form localized states which spread out over energy range due to strong repulsion among the d-electrons themselves. As a consequence, d^n configuration splits into multiplet levels which, in turn, further split by the crystal field such that the '3d' band extends beyond the O(2p)–TM(4s) gap. A number of transitions are therefore possible which may even increase if the selection rules get relaxed due to distortion of oxygen polyhedra. In strontium cobaltite prepared in this work, cobalt exists in the 3+ and 4+ oxidation states and form octahedra and pyramidal prism with oxygen ions. Also, a small amount of Co_3O_4 present has a normal spinel structure with $3d^7$ Co^{2+} (high spin e_g^2 t_{2g}^5) and Co^{3+} (high spin e_g^2 t_{2g}^4/low spin e_g^0 t_{2g}^6) ions occupying tetrahedral and octahedral sites, respectively. The optical absorption peaks can therefore be assigned transitions as (i) 4.12 eV – ligand metal charge transfer (LMCT) from O^{2-} to Co^{3+}, (ii) 1.90 eV – Co^{3+} octahedral d–d metal charge transfer (MMCT) ($^1T_{1g} \rightarrow {}^1A_{1g}$), (iii) 1.58 eV – Co^{3+} octahedral d–d ($^1A_1 \rightarrow {}^1T_1$), (iv) 1.23 eV – O^{2-} to Co^{3+} (t_{2g}) charge transfer, and (v) 0.87 eV – Co^{2+} tetrahedral d–d or Co^{3+} (HS) d–d charge transfer [45–48]. The absorption curve near 301 nm when extrapolated gives the value of band gap for the strontium cobaltite as ~5.17 eV.

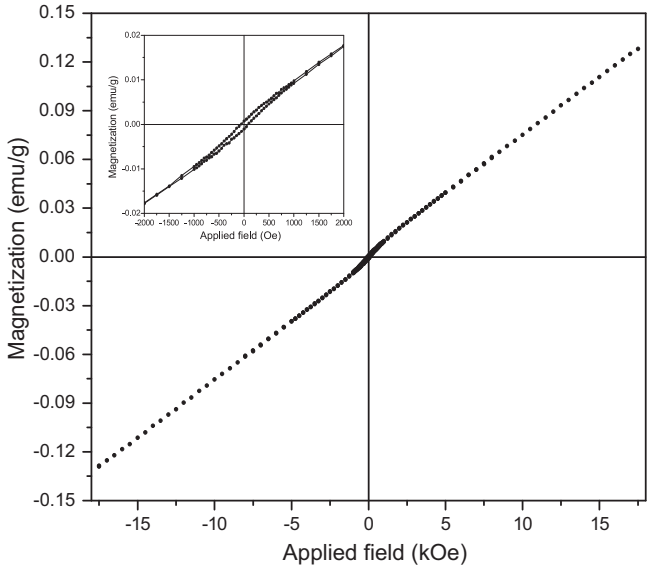

Fig. 4. Magnetization versus field (M–H) plot of strontium cobaltite depicting no saturation; inset shows zoom view of small portion −2 kOe and 2 kOe; depicting hysteresis clearly.

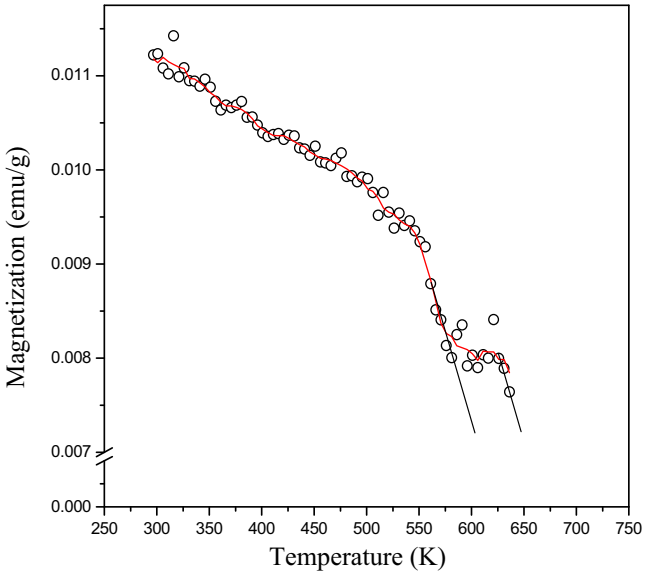

Fig. 5. Magnetization as a function of temperature of strontium cobaltite at a. constant external magnetic field of 500 Oe depicting two ferromagnetic transitions.

3.4. Magnetic behaviour

There is limited work available on the magnetic properties of $SrCoO_{3-\delta}$ system. According to Takeda et al. [24], $SrCoO_{2.5}$ with brownmillerite-type orthorhombic structure exhibits (i) antiferromagnetism with Neel temperature of 570 K, (ii) Co^{3+} ions in high spin state, and (iii) strong superexchange interaction via O^{2-}; exchange integral (J_{ex}) being 28.5k_B with k_B as the Boltzmann constant. On the other hand, Ito et al. [49] investigated the domain wall in the brownmillerite-type $SrCoO_{3-\delta}$ structure with Z – contrast imaging and electron energy loss spectroscopy (EELS) in the scanning transmission electron microscope (STEM) and showed cobalt atoms on octahedral and tetrahedral sites to be in 4+ and 2+ states, respectively. Moreover, Co–O columns in tetrahedral sites are oxygen deficient with ordering of the anion vacancies. Structural relaxation of the CoO_6 octahedra occurs by reduction of the Co^{4+} to Co^{3+} ions with creation of extra oxygen vacancies. According to Taguchi et al. [50], $SrCoO_{2.97}$ possesses spontaneous magnetization of 34 emu/g (or 1.18 μ_B per cobalt atom) at 77 K due to one unpaired electron of Co^{4+} ion in low spin $e_g^0 t_{2g}^5$ state. Another report [22] suggests $SrCoO_3$ to be a ferromagnet with Co^{4+} ions in low spin state and Curie temperature of 222 K. Also, oxygen content (i.e., δ-value) in $SrCoO_{3-\delta}$ strongly influences the magnetic parameters. For example, increase in δ from 0.05 to 0.26 leads to (i) emergence of Co^{3+} (low spin) at the cost of Co^{4+} (low spin) ions and (ii) linear decrease of Curie temperature (T_c) from ~212 to ~178 K, (iii) magnetic moment from ~1.5 to 0.6 when extrapolated to 0 K, and (iv) paramagnetic Curie temperature (θ) from ~270 K to 216 K.

Fig. 4 shows the magnetization versus field (M–H) plot of strontium cobaltite at the room temperature with zoom version of its central portion (field range minus 2 to 2 kOe). Clearly, the hysteresis loop is not saturating but depicts ferromagnetic like nature with low magnetization ~0.128 emu/g (4.4×10^{-3} μ_B per cobalt ion) at 17 kOe, remanent magnetization ~9×10^{-4} emu/g, coercivity ~70 Oe, and loop area ~2.46 emu-Oe/g. The absence of saturation is perhaps due to size distribution of particles and/or inadequacy of magnetic field for causing spin alignment. Fig. 5 shows the variation of magnetization with temperature of strontium cobaltite at a fixed magnetic field of 500 Oe. This reveals continuous decrease of magnetization with temperature and transitions at T_c ~ 750 and 790 K. The corresponding $1/\chi$ versus T plot gives paramagnetic Curie temperatures as ~360 and 417 K, respectively.

3.5. Impedance characteristics

The variation of real part of impedance with frequency of strontium cobaltite at different temperatures shown in Fig. 6(a and b) is used for evaluation of the relaxation frequency of the resistive component. The plots reveal pronounced frequency dependence below 100 kHz, i.e., the magnitude of (Z') decreases with increasing temperature (range 131–161 K) at any given frequency below 100 kHz. Also, at any given temperature, it decreases slowly up to a certain frequency and then rapidly to assume a constant value above 100 kHz. But, the impedance is nearly constant with frequency above 181 K though the value decreases with increase of temperature and lies in the range from 40 to 1 kΩ (Fig. 6a and b). The high value of impedance at low frequencies up to ~10^4 to 10^5 Hz is arising due to the total polarization caused by space charge, dipoles, ions and electrons. The space charge contribution is just the difference in the values of Z' below 10^4 Hz and ~10^5–10^6 Hz when Z' becomes a constant. It may be noticed that the difference is decreasing with increase in the measurement temperature. Obviously, space charge effect reduces significantly with rise in the temperature (Fig. 6a). This leads to relaxation of space charge polarization.

The variation of imaginary part of impedance (Z'') with frequency shown in Fig. 6(c and d) at different temperatures contain a peak above 10 kHz. Also, the peak is shifting towards a higher frequency with rise in the temperature. This behaviour is not observed at higher temperatures as the peaks lie above 10^6 Hz perhaps (Fig. 6d). The nature of curve also indicates the existence of a temperature dependent relaxation process [51]. The frequency corresponding to peak in fact belongs to relaxation process and increases with temperature; the value being 31, 62, and 178 kHz at 131, 141 and 161 K, respectively. Thus, the relaxation time of space charge polarization decreases with rise in temperature and lies in the range ~5–32 μs.

Fig. 7 depicts a typical Cole-Cole (or Z'' versus Z') plot for strontium cobaltite at 161 K. It is composed of two semicircle arcs with their centres lying below the Z'-axis due to contributions from bulk and grain boundaries. The high frequency semicircle (bigger

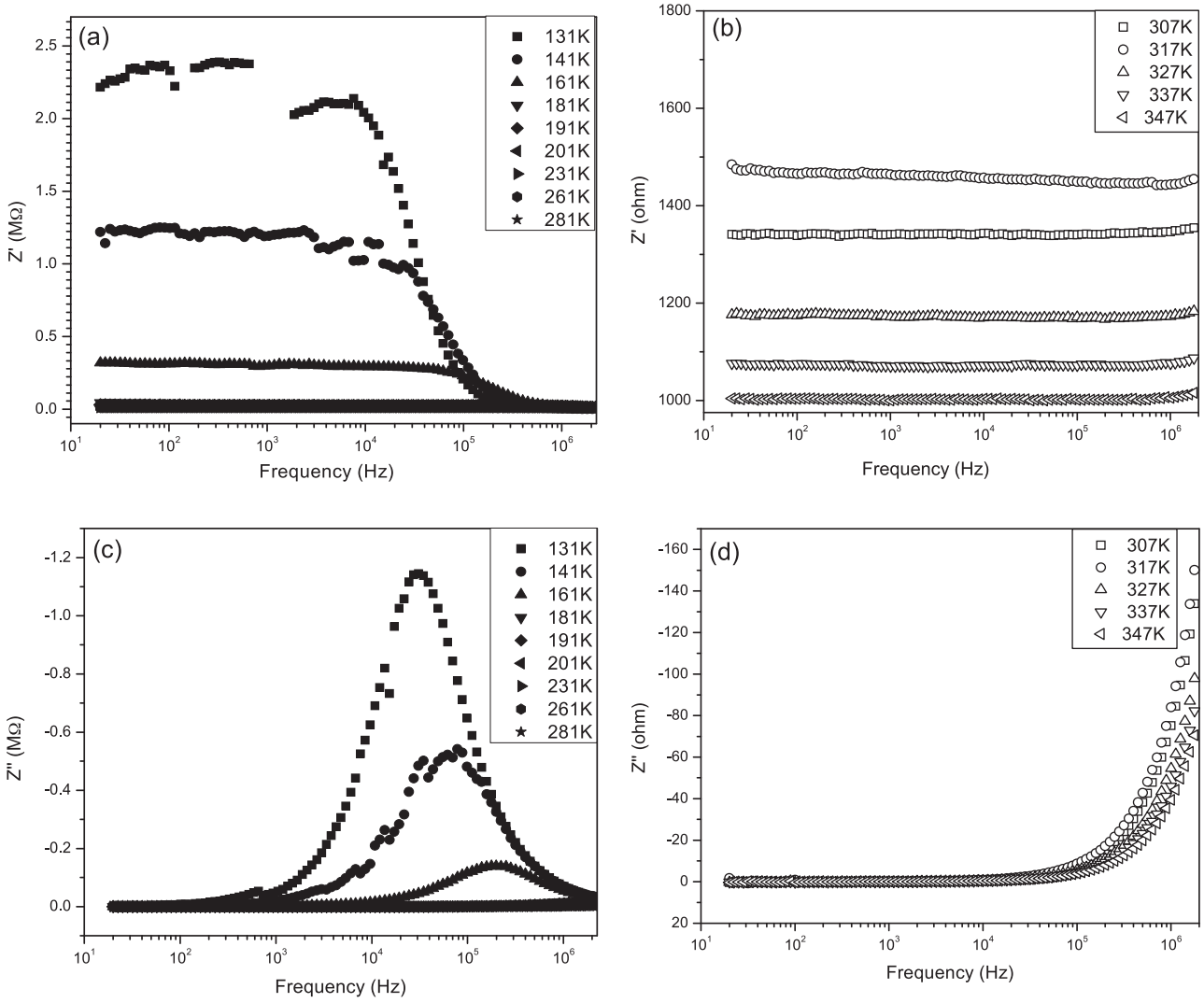

Fig. 6. Variation of impedance Z' (a, b) and Z'' (c, d) as a function of frequency at (a, c). 131–281 K and (b, d) 307–347 K.

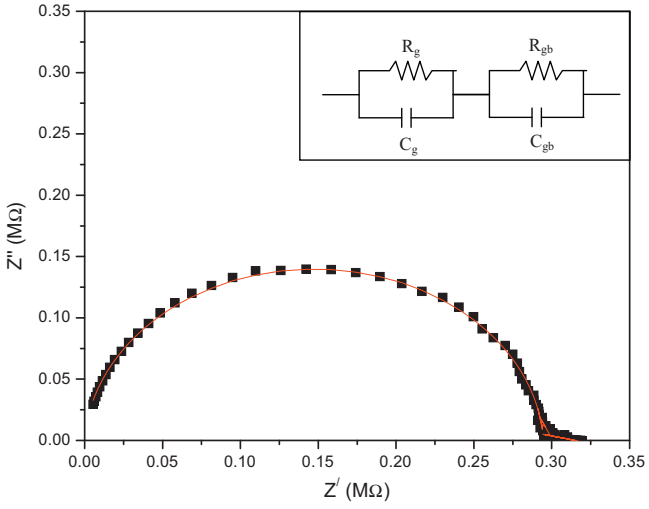

Fig. 7. Cole–Cole plot of strontium cobaltite at 161 K with bigger semicircle fitting. Inset shows combination of two parallel 'RC' circuits corresponding to bulk and grain boundary region.

arc) can be associated with the bulk (grain) property of strontium cobaltite resulting due to parallel combination of resistance (R_b) and capacitance (C_b). Similarly, low frequency semi-circle (smaller arc) can be attributed to grain boundary region with corresponding resistance (R_{gb}) and capacitance (C_{gb}). Thus, the system has two parallel RC circuits joined in series (inset of Fig. 7). The values of R_g and R_{gb} have been obtained from the distance between the two intercepts of the respective arc on the Z'-axis. Since the relaxation time $\tau = (1/\omega)$, where ω is the frequency at the top of the arc, and also $\tau = RC$, capacitance values (C_b and C_{gb}) can be easily deduced. The resistance and capacitance values determined from the two arcs are $R_b \sim 2.95 \times 10^5\ \Omega$, $C_b \sim 20$ pF for bulk and $R_{gb} \sim 2.3 \times 10^3\ \Omega$, $C_{gb} \sim 20$ nF for grain boundaries. Obviously, capacitance of the grain boundary is three orders of magnitude higher than the bulk. This result suggests extensive space charge polarization to prevail at the grain boundaries possibly due to random distribution of comprising ions/groups. With increase in the temperature, the associated polarization effect is subsided progressively.

4. Conclusions

The strontium cobaltite of composition $SrCoO_{3-\delta}$ can be synthesized by decomposition of sol–gel derived oxalate at 1000 °C for

10 h. The product is comprised of (i) dumbbell shape particles of $Sr_6Co_5O_{15}$, exhibiting rhombohedral structure having $a = 6.869$ Å, $\alpha = 87.543^\circ$, $Z = 1$, and space group R32 and (ii) ~7 wt% of Co_3O_4 ($a = 8.0862$ Å) as a secondary phase. It is weakly ferromagnetic with two Curie temperatures (T_C) 750 and 790 K; the coercivity and remanent magnetization at room temperature being 70 Oe and $\sim 9 \times 10^{-4}$ emu/g, respectively. The optical absorption occurring at 4.12, 1.90, 1.58, 1.23 and 0.87 eV can be attributed to ligand metal charge transfer (LMCT) from O^{2-} to Co^{3+}, Co^{3+} octahedral d–d metal metal charge transfer (MMCT) ($^1T_{1g} \rightarrow {}^1A_{1g}$), Co^{3+} octahedral d–d ($^1A_1 \rightarrow {}^1T_1$), O^{2-} to Co^{3+} (t_{2g}) charge transfer, and Co^{2+} tetrahedral d–d or Co^{3+} (HS) d–d charge transfer, respectively. Also, the impedance has a significant contribution from the space charge polarization occurring at grain boundaries; relaxation time being in the range of 5–32 μs.

References

[1] H.J.M. Bouwmeester, A.J. Burggraaf, in: A.J. Burggraaf, L. Cot (Eds.), Fundamentals of Inorganic Membrane Science and Technology, Elsevier, Amsterdam, 1996.
[2] L.W. Tai, M.M. Nasrallah, H.U. Anderson, D.M. Sparlin, S.R. Sehlin, Solid State Ionics 76 (1995) 259–271.
[3] S. Pinitsoontorn, N. Lerssongkram, A. Harnwunggmoung, K. Kurosaki, S. Yamanaka, J. Alloys Compd. 503 (2010) 431–435.
[4] J. Sunarso, S. Baumann, J.M. Serra, W.A. Meulenberg, S. Liu, Y.S. Lin, J.C. Diniz da Costa, J. Membr. Sci. 320 (2008) 13–41.
[5] K.K. Hansen, J. Electrochem. Soc. 157 (9) (2010) P79–P82.
[6] C. Jin, J. Liu, J. Alloys Compd. 474 (2009) 573–577.
[7] X. Wei, T. Wei, J. Li, X. Lan, H. Xiao, Y.S. Lin, Sens. Actuators B 144 (2010) 260–266.
[8] X. Chen, H. Liu, Y. Wei, J. Caro, H. Wang, J. Alloys Compd. 484 (2009) 386–389.
[9] H. Luo, Y. Wei, H. Jiang, W. Yuan, Y. Lv, J. Caro, H. Wang, J. Membr. Sci. 350 (2010) 154–160.
[10] P. Zeng, R. Ran, Z. Chen, W. Zhou, H. Gu, Z. Shao, S. Liu, J. Alloys Compd. 455 (2008) 465–470.
[11] L. Tan, X. Gu, L. Yang, L. Zhang, C. Wang, N. Xu, Sep. Purif. Technol. 32 (2003) 307–312.
[12] J.J. Sprague, O. Porat, H.L. Tuller, Sens. Actuator B 35 (1996) 348–352.
[13] Q. Zhu, T. Jin, Y. Wang, Solid State Ionics 177 (2006) 1199–1204.
[14] F. Zhao, L. Zhang, Z. Jiang, C. Xia, F. Chen, J. Alloys Compd. 487 (2009) 781–785.
[15] I. Park, J. Im, J. Choi, J. Ahn, D. Shin, Solid State Ionics (2010) doi:10.1016/j.ssi.2010.09.017.
[16] R. LeToquin, W. Paulus, A. Cousson, C. Prestipino, C. Lamberti, J. Am. Chem. Soc. 128 (2006) 13161–13174.
[17] X.L. Wang, H. Sakurai, E. Takayama-Muromachi, J. Appl. Phys. 97 (3) (2005), 10M519(1)–10M519(3).
[18] Z.Q. Deng, W.S. Yang, W. Liu, J. Solid State Chem. 179 (2006) 362–369.
[19] C. De la Calle, A. Aguadero, J.A. Alonso, M.T. Fernandez-Dıaz, Solid State Sci. 10 (2008) 1924–1935.
[20] V.M. Tapilin, A.R. Cholach, N.N. Bulgakov, J. Phys. Chem. Solids 71 (2010) 1581–1586.
[21] T. Saitoh, T. Mizokawa, A. Fujimori, M. Abbate, Y. Takeda, M. Takano, Phys. Rev. B 55 (1997) 4257–4266.
[22] H. Taguchi, M. Shimada, M. Koizumi, J. Solid State Chem. 29 (1979) 221–225.
[23] J.C. Granier, L. Fournes, M. Pouchard, Mater. Res. Bull. 21 (1986) 441–449.
[24] T. Takeda, Y. Yamaguchi, H. Watanabe, J. Phys. Soc. Jpn. 33 (1972) 970–972.
[25] L. Elcoro, J.M. Perez-Mato, J. Darriet, A. El Abed, Acta Cryst. B 59 (2003) 217–233.
[26] J.M. Perez-Mato, M. Zakhour-Nakhl, F. Weill, J. Darriet, J. Mater. Chem. 9 (1999) 2795–2808.
[27] K. Iwasaki, M. Shimada, H. Yamane, J. Takahashi, S. Kubota, T. Nagasaki, Y. Arita, J. Yuhara, Y. Nishi, T. Matsui, J. Alloys Compd. 377 (2004) 272–276.
[28] K. Iwasaki, Ito Tsuyoshi, T. Matsui, T. Nagasaki, Ohta Shingo, K. Koumoto, Mater. Res. Bull. 41 (2006) 732–739.
[29] M.-H. Whangbo, H.-J. Koo, K.-S. Lee, O. Gourdon, M. Evain, S. Jobic, R. Brec, J. Solid State Chem. 160 (2001) 239–246.
[30] J.E. Saal, Y.W. Wang, S. Shang, Z.K. Liu, Inorg. Chem. 49 (2010) 10291–10298.
[31] K. Iwasaki, H. Yamane, T. Murase, M. Yoshino, T. Ito, T. Nagasaki, Y. Arita, T. Matsui, J. Ceram. Soc. Jpn. 117 (1) (2009) 89–93.
[32] J. Sun, G. Li, Z. Li, L. You, J. Lin, Inorg. Chem. 45 (2006) 8394–8402.
[33] K. Iwasaki, T. Murase, T. Ito, M. Yoshino, T. Matsui, T. Nagasaki, Y. Arita, Jpn. J. Appl. Phys. 46 (2007) 256–260.
[34] T. Takami, M. Horibe, M. Itoh, J. Cheng, Phys. Rev. B 82 (6) (2010), 085110(1)–085110(6).
[35] J. Jung, S.T. Misture, D.D. Edwards, Solid State Ionics 181 (2010) 1287–1293.
[36] W.T.A. Harrison, S.L. Hegwood, A.J. Jacobson, J. Chem. Soc. Chem. Commun. 19 (1995) 1953–1954.
[37] J.A. Campa, E. Guitierrez-Puebla, M.A. Monge, I. Rasines, C. Ruiz-Valero, J. Solid State Chem. 108 (1994) 230–235.
[38] H. Watanable, T. Takeda, Proc. Int. Conf. Ferrites, Japan, 1970, p. 598.
[39] T. Takeda, H. Watanable, J. Phys. Soc. Jpn. 33 (1972) 973–978.
[40] J.C. Granier, S. Ghodbane, Mater. Res. Bull. 14 (1979) 831–839.
[41] J. Rodriguez, J.M. Gonzalez Calbet, Mater. Res. Bull. 21 (1986) 429–439.
[42] Y. Takeda, R. Kanno, T. Takada, O. Yamamoto, M. Takano, Y. Bando, Z. Anorg, Allg. Chem. 540–541 (1986) 259–270.
[43] V.V. Vashook, M.V. Zinkevich, G. Yu, Zonov Solid State Ionics 116 (1999) 129–138.
[44] J. Rodriguez, J.M. Gonzalez, J.C. Greneir, J. Pannetier, M. Anne, Solid State Commun. 62 (1987) 231–234.
[45] M. Lenglet, C.K. Jorgensen, Chem. Phys. Lett. 229 (1994) 616–620.
[46] J.W.D. Martens, W.L. Peeters, H.M. Van Noort, M. Erman, J. Phys. Chem. Solids 46 (1985) 411–416.
[47] K.M.E. Miedzinska, B.R. Hollebone, J.G. Cook, J. Phys. Chem. Solids 48 (1987) 649–656.
[48] M. Lenglet, B. Lefez, Solid State Commun. 98 (1996) 689–694.
[49] Y. Ito, R.E. Klie, N.D. Browing, T.J. Mazanec, J. Am. Ceram. Soc. 85 (2002) 969–976.
[50] H. Taguchi, M. Shimada, F. Kanamaru, M. Koizumi, Y. Takeda, J. Solid State Chem. 18 (1976) 299–302.
[51] A.K. Jonscher, Nature 267 (1977) 673–679.